Article

A Manual and Machine Learning Based Case Investigations for detecting the lymphatic spread of canine cancers

Dr. Anjan Sahoo , Kanchan Lata Kashyap [*] , Dr. Nilamadhab Mishra , Dr.Indramani Nath , Dr. Susen Panda , Dr. Sanghamitra Pati , Budheswar Dehur

Article

A Manual and Machine Learning Based Case Investigations for Detecting the Lymphatic Spread of Canine Cancers

Anjan Kumar Sahoo [1], Kanchan Lata Kashyap [2,*], Nilamadhab Mishra [3], Indramani Nath [4], Susen Kumar Panda [5] and Sanghamitra Pati [6] and Budheswar Dehur [7]

[1] Department of Veterinary Surgery and Radiology, College of Veterinary Science and AH, OUAT, Bhubaneswar-751003; aks76vet@gmail.com
[2] SCSE, VIT Bhopal University, India
[3] SCSE, VIT Bhopal University, India; nmmishra77@gmail.com
[4] Department of Veterinary Surgery and Radiology, College of Veterinary Science and AH, OUAT; indravet@yahoo.co.in
[5] Department of Veterinary Pathology, College of Veterinary Science and AH, OUAT; drsusen_panda@yahoo.com
[6] ICMR-Regional Medical Research Institute, Chandrasekharpur, Bhubaneswar-751 023; sanghamitra.pati@icmr.gov.in
[7] ICMR-Regional Medical Research Institute, Chandrasekharpur, Bhubaneswar-751 023; budheswar.dehuri@gmail.com
*   Correspondence: kanchan.k@vitbhopal.ac.in

Abstract: The objective of the current investigation is to identify the first or first draining node or sentinel lymph node (SLN) from the primary tumor mass in a regional lymphocenter. Four different indirect lymphography (IL) methods were employed in 96 canine patients with different types of cancer between 2018 and 2021. The IL technique involved intradermal, submucosal, and peritumoral injections of 2ml contrast agent in the four-quadrant principle which were divided into equal aliquots. Lymphatic mapping with lipiodol (iodized oil) was 100% in squamous cell carcinoma of the head and neck, anal sac apocrine gland adenocarcinoma, mast cell tumor, squamous cell carcinoma of the skin, mammary carcinoma, and with methylene blue dye, 100% detection was achieved in testicular tumor and mammary carcinoma. Instead of a very short washout time of 2 minutes, Iohexol showed an excellent detection in indirect CT lymphography for histiocytic sarcoma and in indirect radiographic lymphography for lymphosarcoma. The significance of contrast and blue dyes in detecting the lymphatic spread of canine cancers is clearly emphasized in the current investigation. The nature of cancerous tissue was again analyzed through image and machine learning approach in this work. Supervised machine learning technique is applied in this work for automatic classification of cancerous and non-cancerous regions. Various statistical and texture-based features are extracted from X-Ray images and support vector machine with linear, polynomial, multilayer perceptron (MLP), and RBF kernel functions are applied for classification. Highest 95.53%, 94.64%, 93.05% sensitivity, specificity, accuracy, respectively, is achieved using RBF kernel function.

Keywords: Lipidol ultrafluid; Methylene blue; Iohexol; Lymphography; Supervised machine learning; Gray level Co-occurrence matrix

1. Introduction

Tumor metastasis, primarily involves the lymphatic pathway and in this lymph nodes of regional lymphocenter plays a vital role. Both direct lymphography and indirect lymphography techniques can be used to visualize these lymphatic pathways and lymph nodes (Mayer *et al.*,2013; Brissot and Edery, 2016). Evaluation of a lymph node can be done clinically by using palpation, LN measurement (Beer *et al.*,2018; Fournier *et al.*, 2018), FNAC (Fournier *et al.*, 2018; Karakitsou *et al.*, 2022), ultrasonography (Beer *et al.*,2018; Chiorean *et al.*, 2016; Sahoo *et al.*, 2021a), and histopathology

(Sledge *et al.*, 2016). Accurate assessment of the locoregional metastases is aided by the identification of initial draining LN or echelon nodes, or SLN in a regional lympho center (Morton *et al.*, 1992; Skinner et al., 2017; Skinner *et al.*, 2018, Sahoo et al., 2021b). Currently, several IL methods are used for assessing the lymphatic and lymph nodes draining the primary tumor mass. Those are vital blue dyes for visual detection (Mayer *et al.*,2013; Brissot and Edery, 2016), radiocolloid lymphoscintigraphy (Hlusko *et al.*, 2020; Manfredi *et al.*, 2021), radiographic lymphography (Mayer *et al.*,2013; Lee *et al.*, 2018; Collivignarelli *et al.*,2021), computed tomography (CT), lymphography (Sarowitz *et al.*, 2017; Grimes *et al.*, 2017;Majeski *et al.*, 2017; Rossi *et al.*,2018; Lapsley *et al.*, 2020), fluorescent optical imaging or Near-infrared imaging (NIR)(Iida *et al.*, 2913; Wan *et al.*,2021; Beer *et al.*,2022), contrast-enhanced ultrasound (CEUS)(Gelb *et al.*,2010; Fournier *et al.*, 2020), photoacoustic imaging(Garcia-Uribe *et al.*, 2015), SPECT/PET CT(Beer *et al.*, 2018; LeBlanc *et al.*, 2013), Magnetic resonance (MR) lymphography (Turkbey *et al.*, 2015), hybrid tracer (Nyberg *et al.*, 2011), and nanocarriers (Jain *et al.*, 2009). Manual detection of various types of cancerous tissues of canine patients is tedious process. Image processing and machine learning plays an important role for automatic detection of cancerous tissues. Automatic cancer detection system can be developed by applying image processing and machine learning techniques. Doctors can use automated system to take second opinion regarding this disease. Deep learning based VGGNet-16 along with support vector machine and random forest techniques are applied for classification of canine mammary tumor by using histopathological images (Kumar *et al.*, 2020). Authors achieved highest 97% accuracy with VGGNet-16. Machine learning technique is applied to detect liver tumor of dogs by extracting texture features of CT-scan images (Shaker *et al.*, 2021). They obtained 90%, 67%, and 100% accuracy, sensitivity, and specificity, respectively. The goal of present research is to validate the identification of tumor and lymph nodes with those analyzed through preliminary machine learning approach.

Major Highlights of Present work

- Indirect lymphography technique using three contrast agents viz. Iohexol, Lipiodol, and Methylene blue (MB) detects Sentinel lymph node (SLN) in canine solid tumors.
- SLN detected in buttock sarcoma, cutaneous histiocytic sarcoma for the first time. Immunostaining of inguinal lymph node (LN) detects Lipiodol after one month, which clearly indicates its lymphotropic nature.
- Lipiodol showed highest detection rate in skin tumors of forelimb, hind limb, and mammary gland whereas MB is very good in intraoperative SLN detection in mammary carcinoma.
- Automatic cancer detection and classification system of canine patients is developed by applying image processing and supervised machine learning technique. Various statistical and texture-based features are extracted from X-Ray images and support vector machine with linear, polynomial, multilayer perceptron (MLP), and RBF kernel functions are applied for classification.

2. Material and Methods

The present study described 96 clinical cases of client-owned dogs with primary tumor masses referred to the department of Surgery, between October 2018 and February 2021.The study was approved by institutional animal ethical committee (IAEC). The various steps followed for this study is given in the following subsections.

2.1. Preclinical work up and clinical staging

Preclinical workup and clinical staging of all patients were done by physical examination, clinical symptoms, radiography, ultrasound scanning (GE Healthcare, Ireland), blood biochemistry, cytology (FNAC or impression smear), tissue biopsy or histopathology, CT scan of the tumor and lymph node.

2.2. Sentinel lymph node (SLN) Localization

Localization of SLN is performed through four types of IL technique:

i.   indirect radiographic lymphography with Lipiodol Ultra-Fluid™ (iodized ethyl-esters of the fatty acids of poppy seed oil, an oil-based nonionic iodine contrast agent, Guerbet, Aulnay-sous-bois, France; 480 mg iodine per ml).

ii.   IL with methylene blue (MB) dye (5mg/ml)

iii.   indirect radiographic lymphography with Omnipaque300 (Iohexol – a water-soluble nonionic iodine contrast agent (300mgI/ml), GE Healthcare, USA),

iv.   iohexol-based indirect CT lymphography. Brief description of each technique is given in next subsections.

(i) Indirect radiographic lymphography with Lipiodol Ultra-Fluid

Indirect radiographic lymphography was performed with intradermal/submucosal injection of 2ml Lipiodol with a tiny gauge needle (24G needle or insulin syringe) in four-quadrant principle (at 12, 3, 6 and 9 o'clock position and dispersed in equal aliquot @ 0.5mL per site) at the peritumoral site, accomplished in a slow rate (at 2mL/min). Two orthogonal views (lateral and ventrodorsal views) of radiography images are recorded at intervals of 30 minutes, an hour, and 24hours following contrast injections to observe the uptake by first lymph node.

(ii) Indirect lymphography with methylene blue dye

IL with MB dye (5mg/mL) is performed intradermally/subcutaneously and peritumorally in four-quadrant principle (equal aliquot of 0.5mL/site) using a 24G needle or insulin syringe, intraoperatively within 0.5 cm from primary tumor mass, and surgery began 10-15 min afterwards. The superficial lymphatic pathway from the injection site to the first draining LN was identified by dissecting skin flaps and monitoring the flow of dye. Visual evaluation of in vivo MB uptake indicated that nodes with dark blue coloring are acceptable, very pale blue coloration was fair, and absence of coloration or non-identification was unsatisfactory.

(iii) Indirect radiographic lymphography with omnipaque-300 (iohexol)

Indirect radiographic lymphography with iohexol was performed in a similar four-quadrant concept (0.5mL per site) with a 22G 5mL syringe, with injections made intradermally and peritumorally at a distance of 0.5cm from the original lesion. To see how iohexol moved through the lymphatic system and into the first draining lymph node, digital radiography images were taken immediately after the injection (0 to 2 minute), then at 3, 5, 10, and 20 minutes.

(iv) Indirect CT lymphography with iohexol

For indirect CT lymphography, patients were sedated on the CT table with injection Atropine sulphate (0.04 mg/Kg body weight) and injection Tiletamine, Zolazepam (Zoletil®, Virbac NZ) @ 10 mg/kg body weight). Precontrast CT study of the abdomen and pelvis was performed with 2.0 to 5.0-mm slices thickness in a 16- slice Siemen's CT scanner. Technical settings were kept as 120-150 kV, mAs 60-200,512x 512 matrix, 250-500 mm field of view. Subsequently, Indirect CT lymphography is conducted via peritumoral injection (subcutaneous injection) of 2mL of iohexol in four-quadrant concept. CT scan was taken immediately after injection and then every 1, 3, 5, 10 min until the enhanced lymph nodes are visible. Medical image viewing software was used to measure images in DICOM format. A first-tier node, also referred to as an echelon node, is the node inside the regional lymphocenter that received the initial uptake of contrast material.

2.3. Automatic classification of cancerous and non-cancerous images using Machine learning technique

In this step, X-Ray images are used for automatic classification of cancerous and non- cancerous regions by applying machine learning techniques. The 300 regions are cropped from collected images which include 160 cancerous and 140 non-cancerous regions. Next, feature extraction is performed to characterize the cropped regions. Finally, support vector machine is used for classification of images as cancerous or non-cancerous. The description of extracted features and classifiers are given in next sub-sections.

2.4. Feature Extraction

Textural features play an important role to extract the meaningful information from the gray scale images. Texture features contain spatial relationship among pixels and gray value variations in the suspicious region. First order statistical and GLCM features are used to detect the cancerous regions in X-ray images.

2.5. First Order Statistical Features

Six first order statistical features namely mean, average contrast, skewness, kurtosis, energy and entropy are extracted from the suspicious ROI (Materka *et al. 1973*) For an image with probability density of intensity levels $p(i)$ and maximum gray levels M, these features are expressed as:

Mean represents the average intensity value of image.

$$Mean\ (\mu) = \sum_{i=0}^{M-1} ip(i) \tag{1}$$

Average contrast gives intensity variation around the mean.

$$Averagecon\ trast\ (\sigma^2) = \sum_{i=0}^{M-1} (i-\mu)^2\ p(i) \tag{2}$$

Skewness measures the histogram asymmetry around the mean.

$$Skewness(\mu^3) = \sigma^{-3} \sum_{i=0}^{M-1} (i-\mu)^3\ p(i) \tag{3}$$

Kurtosis represents the flatness of histogram.

$$Kurtosis\ (\mu^4) = \sigma^{-4} \sum_{i=0}^{M-1} (i-\mu)^4\ p(i) - 3 \tag{4}$$

Energy is calculated as

$$Energy\ (E) = \sum_{i=0}^{M-1} [ip(i)]^2 \tag{5}$$

Entropy indicates the randomness of intensity value of image.

$$Entropy = -\sum_{i=0}^{M-1} p(i)\log(p(i)) \tag{6}$$

The probability density of intensity levels $p(i)$ is calculated by

$$p(i) = \frac{g(i)}{N}, \tag{7}$$

where $g(i)$ is total number of pixels with intensity value i and N is the total number of pixels in the image.

2.6. Gray Level Co-occurrences Matrix Features (GLCM)

GLCM gives the second-order features to generate texture attributes (Haralick *et al.*1973*). GLCM represents distribution of intensities and the information about the relative positions of neighboring pixels of an image. The elements of GLCM represent the joint probabilities $C(i,j)$ of all pair wise

combinations of gray level i and j. These pairs should be separated by a distance d in the given orientation θ of a spatial window. The elements of GLCM can be represented as:

$$C(i,j) = \frac{g(i,j)}{\sum\limits_{i=1}^{M}\sum\limits_{j=1}^{M} g(i,j)}, \tag{8}$$

where, M denotes total number of gray levels, $g(i,j)$ represents number of occurrences of gray levels i and j within given spatial window in given pair (d,θ).

$g_x(i) = i^{th}$ entry in marginal probability matrix obtained by summing the rows of $\sum\limits_{j=1}^{2M} g(i,j)$

$$g_y(j) = \sum\limits_{i=1}^{2M} g(i,j) \tag{9}$$

$$g_{x+y}(k) = \sum\limits_{i=1}^{M}\sum\limits_{j=1}^{M} g(i,j) \tag{10}$$
here, $i+j = k = 2,3,..2M$

$$g_{x-y}(k) = \sum\limits_{i=1}^{M}\sum\limits_{j=1}^{M} g(i,j) \tag{11}$$
here $|i-j = k = 0,1,...M-1|$

Assuming $\sum\limits_{i} = \sum\limits_{i=1}^{2M}$ and $\sum\limits_{j} = \sum\limits_{j=1}^{2M}$

Fifteen GLCM features extracted from the segmented regions are represented as:

Energy, also known as uniformity or angular second moment, measures the textural uniformity, i.e., pixel pair repetitions.

$$Energy = \sum\limits_{i}\sum\limits_{j} g_{ij}^2 \tag{12}$$

Entropy measures the randomness of an image. It is large when the image is not texturally uniform.

$$Entropy = -\sum\limits_{i}\sum\limits_{j} g_{ij} \log g_{ij} \tag{13}$$

Contrast measures the intensity difference between a pixel and its neighbor over the entire image.

$$Contrast = \sum\limits_{i}\sum\limits_{j} (i-j)^2 g_{ij} \tag{14}$$

Correlation measures how the pixel is correlated to its neighbors over the entire image.

$$Correlation = \frac{\sum\limits_{i}\sum\limits_{j}(ij)g(ij)\mu_x\mu_y}{\sigma_x\sigma_y}, \tag{15}$$

where μ_x, μ_y, σ_x, and σ_y denote means and standard deviations of marginal probability matrix of g_x and g_y respectively.

Autocorrelation provide a measure of gray-tone dependencies in the image.

$$Autocorrelation = \sum\limits_{i}\sum\limits_{j} (ij)g(i,j) \tag{16}$$

Maximum probability measures the strongest response of co-occurrence matrix.

$$Maximum probability = \max_{i,j} g(i,j) \tag{17}$$

Homogeneity, also known as inverse difference moments, measures the spatial closeness of the distribution of elements in co-occurrence matrix diagonally.

$$Homogeneit\,y = \sum_i \sum_j \frac{1}{1+(i-j)^2} g_{ij} \tag{18}$$

Variance measures image heterogeneity and is strongly correlated to standard deviation. It increases when the gray values differ from their mean.

$$Variance\ (\text{var}) = \sum_i \sum_j (i-\mu)^2 g_{ij} \tag{19}$$

The following features are secondary and defined in terms of the features discussed above:
Sum average is obtained from the pixel in consideration and the size of gray scale.

$$SumAverage\,(sa) = \sum_{i=2}^{2M} i g_{x+y}^{(i)} \tag{20}$$

Sum Entropy is calculated as the logarithmic function of the image in consideration.

$$sumEntropy\,(se) = -\sum_{i=2}^{2M} g_{x+y}^{(i)}(i)\log\{g_{x+y}(i)\} \tag{21}$$

Sum Variance is calculated from the original image and the sum entropy (se).

$$SumVariance(sv) = \sum_{i=2}^{2M} (i-se)^2 g_{x+y}(i) \tag{22}$$

Difference Entropy measures non-uniformity when difference measure obtained from the original image is considered.

$$Difference\ Entropy\ = -\sum_{i=0}^{M-1} g_{x-y}^{(i)}(i)\log\{g_{x-y}(i)\} \tag{23}$$

Difference Variance is a variance measure between image intensities calculated as a function of the sum entropy (se).

$$Difference\ Variance\ = \sum_{i=2}^{2M} (i-se)^2 g_{x-y}(i) \tag{24}$$

Information Measure of Correlation1 (IMC1)

$$IMC1 = \frac{HXY - HXY1}{\max\{HX, HY\}} \tag{25}$$

Information Measure of Correlation2 (IMC2)

$$IMC2 = \sqrt{1-\exp[-2.0(HXY2 - HXY)]}, \tag{26}$$

where
$$HXY = -\sum_i \sum_j g_{ij}\log_2 g_{ij} \tag{27}$$

$$HXY1 = -\sum_i \sum_j g_{ij}\log\{g_x(i)g_y(j) \tag{28}$$

$$HXY2 = -\sum_i \sum_j g_x(i)g_y(j)g_{ij}\log\{g_x(i)g_y(j)\} \tag{29}$$

2.7. Classification

SVM is used to discriminate cancerous and non-cancerous regions. It is a supervised machine learning technique which creates the hyper-plane to separate the objects of different classes (Cortes *et al*. 1995). It creates support vectors to identify the boundaries between two classes. The optimal position of the hyper-plane is determined by the support vector. Suppose $x = \{x_i | i = 1,2,...,N\}$ represents a training set of N feature vectors in d dimensional feature space and $y_i \in (-1,+1)$ represents the class labels associated with x. Normal and abnormal tissues are denoted by class label +1 and -1, respectively. Linear separable feature vector is accomplished by defining a hyper-plane as:

$$w.x_1 + b \geq +1 \quad \text{for} \quad y_i = +1 \tag{30}$$

$$wx_1 + b \leq -1 \quad \text{for} \quad y_i = -1, \tag{31}$$

where w is normal to the hyper plane and b is threshold parameter. Generalized form of these equations can be expressed as:

$$y_i(wx_i + b) \geq 1 \quad \text{for} \quad i = 1,2,3,...,N \tag{32}$$

Distance between two hyper planes is given as $\frac{2}{|w|}$. Better separation can be achieved between two classes for the optimized (maximum) value of the distance of two hyper planes. Maximum distance between two hyper planes is inversely proportional to $|w|$. Lagrangian function is used to obtain maximum distance and can be expressed as:

$$f(x) = \sum_{i=1}^{N} \alpha_i w_i(x_i.x) + b, \tag{33}$$

where α_i is a lagrangian multiplier of dual optimization problem that explains separating hyperplane $w_i(x_i.x)$. x is classified as member of the positive class for all values of $f(x) \geq 0$; otherwise it belongs to the negative class. The simplest way to separate two groups of data is with straight line (1-dimensional), flat-plane (2 dimensional) and N-dimensional hyper-plane. In many situations non-linear regions can separate the data more efficiently. SVM handles this situation by applying kernel function to map the data into different feature space where hyperplane is unable to group the data. SVM transform the data into higher dimensional feature space where linear separability is possible by applying kernel trick. SVM use various kernel functions such as linear, polynomial, RBF and MLP (Sigmoid) which are mathematically represented as:

Kernel Function ($K(x_i,x_j)$)	Mathematical Description
Linear	$x_i.x_j$
Polynomial	$(\gamma x_i.x_j + C)^d$
RBF	$\exp(-\gamma|x_i - x_j|^2)$
MLP	$\tanh(\gamma x \cdot x_j + C)$

8

where, γ is adjustable parameter, C is capacity constant, d is order of polynomial, and $K(x_i, x_j) = \phi(x_i) \cdot \phi(x_j)$, i.e., kernel function represents a dot product of data points mapped into higher dimensional feature space by transformation ϕ.

3. Results

Four types of indirect lymphography (IL) technique was used for detection of sentinel lymph node in seven major cancer types: (i) oral and maxillofacial cancer in 14 subjects, (ii) anal sac tumors in 14 subjects, (iii) cancer of the skin and subcutis in 20 subjects, (iv) soft tissue sarcoma in 14 subjects, (v) lymphosarcoma in 6 subjects, (vi) cancer of male genital system in 5 subjects, and (vii) mammary carcinoma in 23 subjects. Four types of IL methods effectively detect SLNs in oral squamous cell carcinoma, fibromatous epulids, oral and maxillofacial osteosarcoma, ossifying epulids, and basal cell carcinoma.

When injections are performed submucosally within 0.5cm from the tumor margin of oral SCC along with messaging in the direction of lymphatic flow, Lipiodol Ultrafluid successfully localize the mandibular lymph node in 6 subjects as SLN within 24 hours as shown in Fig.1. SLN (Mandibular LN) is discovered after 24 hours; when, the injection site is subcutaneous and more than 0.5cm from the underlying tumor (oral SCC). Out of 14 cases, SLN is identified in 10 cases, with 8 of them are found positive for metastases through biopsy, and 3 cases of SCC had a recurrence.

Figure 1. lymphatic drainage pathway (white line) from oral squamous cell carcinoma (primary lesion) to Mandibular lymph node (Sentinel lymph node).

Out of 14 cases in perianal tumors (anal sac apocrine gland adenocarcinoma (ASAGAC) (n=11) and perianal gland adenocarcinoma (n=3), IL with MB is performed in 3 cases, IL with iohexol in 3 cases, and IL with Lipiodol in 8 cases. The medial iliac lymph node (n=4) is detected as the SLN for these cancers, when mapping is done with Lipiodol as shown in Fig. 2. Ultrasound-guided biopsy of miLN yields positive for metastases (n=2) which is a negative prognostic indicator. Closed anal sacculectomy and histopathology identify a solid type of ASAGAC (n=8).

Figure 2. Medial iliac lymph node as SLN in Anal Sac apocrine gland adenocarcinoma.

SLN mapping for 20 primary tumors (MCT-11, SCC-3, basal cell carcinoma-1, canine papillomatosis-3, cutaneous plasmocytoma-1, sebaceous gland adenocarcinoma-1) of skin and subcutaneous tissue is performed with four IL methods. MCT weighing 7.8 kg, 3kg, 1.9kg, 1.8kg, 300g, 250g, and lymph nodes weighing 3g, 5g, 10g, up to 90g are excised through *en bloc* surgical resection with a broad margin. According to the Patnaik grading system (Patnaik *et al.*, 1984), the clinical staging of 11 MCT is Grade III (n=5), Grade II (n=3), and Grade I (n=3). In MCT(n=11), IL with Lipiodol results in 100% detection rate. SLN are detected within 24hr of injections along with gentle messaging in Lipiodol whereas 2 min of injection in iohexol(n=2). Six of the 15 SLN, discovered through cytology and biopsy are determined to be non-metastatic, whereas the other 9 are found to be positive for metastasis. IL was unable to detect any lymph node in rest 5 cases. The SLN for tumors in the front leg is the cervical lymph node as shown in Fig.3.
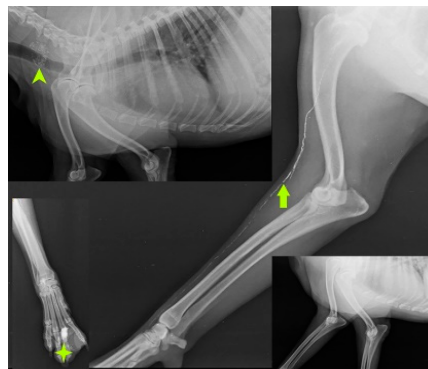

Figure 3. Cervical lymph node (arrow head) as sentinel lymph node for mast cell tumor (solid star) of front leg.

IL with MB employed in the second digit of the right front leg with recurrent MCT perioperatively and cervical lymph node stained blue within 10-15 min of injection as shown in Fig. 4.

Figure 4. cervical LN (inset mass) as SLN detected using MB dye in front leg.

Injections of iohexol into the MCT of the hind leg immediately identify popliteal LN as SLN within 1-2 min. Indirect CT lymphography with iohexol in MCT of upper thigh detects inguinal LN as SLN and miLN as second-tier node in 2 min of intradermal and peritumoral injection in MCT of the hindleg as shown in Fig. 5.
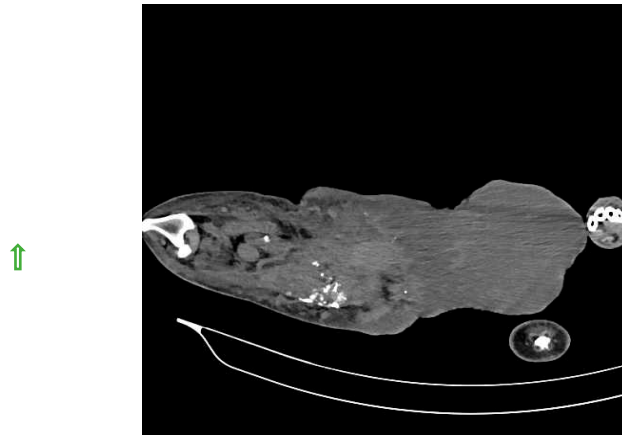
10

Figure 5. Inguinal LN (contrast enhanced pointing arrow) was detected as SLN in MCT of right upper thigh.

To prevent any sort of allergic reaction and mast cell activation in the case of multiple MCT, only IL with iohexol was used. In SCC of hindleg, Popliteal LN (PoLN, Patchy contrast uptake) was localized as SLN within 24 hours of Lipiodol injection as shown in Fig. 6 and PoLN was also found positive for metastases on biopsy.

Figure 6. Popliteal LN (PoLN, Patchy contrast enhanced) as SLN in hindleg SCC.

SLN was detected in histiocytic sarcoma (n=4) and buttock sarcoma (n=3) only, and not localized in other soft tissue sarcoma (n=7) (lipoma, liposarcoma, infiltrative lipoma, cavernous hemangioma and cutaneous fibrosarcoma). Indirect CT lymphography with iohexol injection in histiocytic sarcoma detects inguinal LN as SLN (Figure 7) and miLN as a second-tier node within 2 min, and the inguinal node is found metastasis-free on cytology and biopsy.
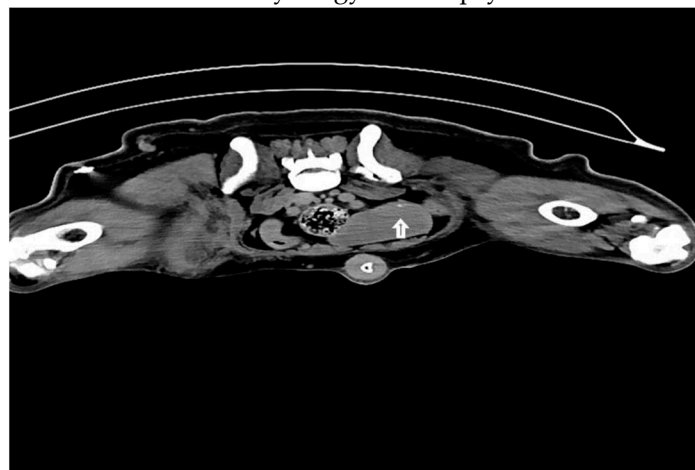
Figure 7. Inguinal LN as SLN in histiocytic sarcoma detected through indirect CT lymphography with iohexol.

IL with Lipiodol in recurrent buttock sarcoma (operated six times) detects lymphatic flow to right inguinal LN only after 24 hours and to miLN after 48 hours as shown in Fig. 8. The opacity was noticeable upto 28 days of injection.
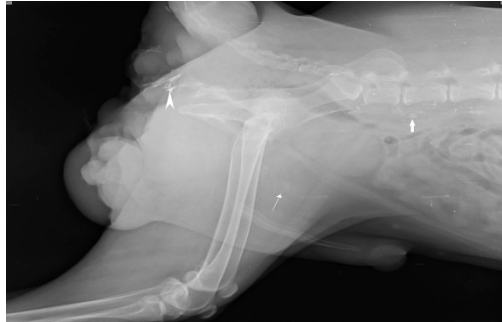

Figure 8. Inguinal LN (plain arrow) as SLN for buttock sarcoma detected through IL with Lipiodol and miLN (solid arrow) is the second-tier node.

In multicentric lymphosarcoma (n=6), within minutes of peritumoral and intradermal injection of iohexol in popliteal LN, deep inguinal LN and miLN were discovered as SLN as shown in Fig. 9.
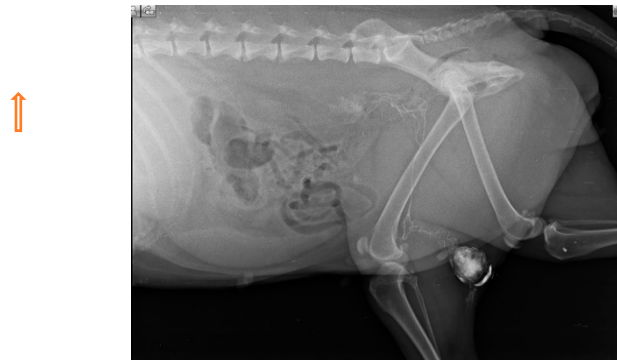

Figure 9. Lymphatic channel from popliteal lymph node to inguinal lymph node and then to medial iliac lymph node (solid white arrow) in multicentric lymphosarcoma.

The malignancy criteria of the peripheral LN (submandibular, parotid, cervical, axillary, inguinal, and popliteal LN) were clearly described by ultrasonography. These criteria include oval form with S/L ratio 1, peripheral and central vascularization, and hypoechoic nodes as shown in Fig. 10, which are confirmed by cytology and biopsy. In the case of a primary tumor mass (lymphoma at 3rd molar) in the mouth cavity, mandibular LN were recognized as SLN within 2 minutes of indirect CT lymphography with iohexol. All superficial LN were found to have metastasized in lymphosarcoma which was a poor predictor of survival time.
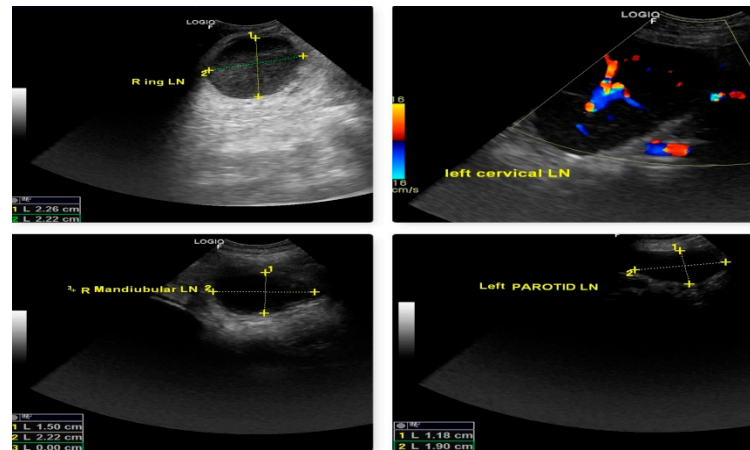
Figure 10. Malignant changes observed through B-mode USG and color Doppler as generalized lymphedema (hypoechoic texture with S/L ratio ≤ 1, peripheral and central vascularization) in lymphosarcoma (ocular form).

The SLN for cancers of the male genital system (n=5) was the inguinal LN (TVT, mixed germ cell-stromal cell tumor). Within 10 minutes of intradermal and peritumoral MB dye injection, progression of the blue-stained lymphatic channel from the primary tumor mass (testicular tumor, mixed germ cell-stromal cell tumor) to the inguinal LN (enlarged, hard, fixed, and bilateral) is seen as in Fig. 11. Metastasis was detected in the excised inguinal LN by cytology. In TVT (n=2), within 2 minutes of injection, IL with iohexol detects inguinal LN as SLN in two cases, however those cases have not shown evidence of metastasis.

Figure 11. Flow of MB dye through blue stained lymphatic from testicular tumor to inguinal LN (SLN).

Out of 23 cases of mammary carcinoma, IL with MB dye procedure detects 12 SLN, IL with Lipiodol detects 9 SLN and IL with iohexol is able to detect SLN in 2 cases. Carcinoma was found in both sides from 2nd to 5th mammary gland (MG) but not in 1st MG. Preoperative IL with Lipiodol injection was performed in 9 primary mammary carcinomas via intradermal and subcutaneous routes, led to localization of nine SLN (lymphoid plexus of thigh –two, inguinal-four, axillary –two, and sternal-one). IL with Lipiodol in mammary carcinoma of 2nd MG and subsequent radiograph after 24hour detected sternal lymph node as SLN and axillary LN as second tier node after 48hour is shown in Fig. 12. Post injection radiographs are monitored in 5 patients up to 21 days with similar LN visibility
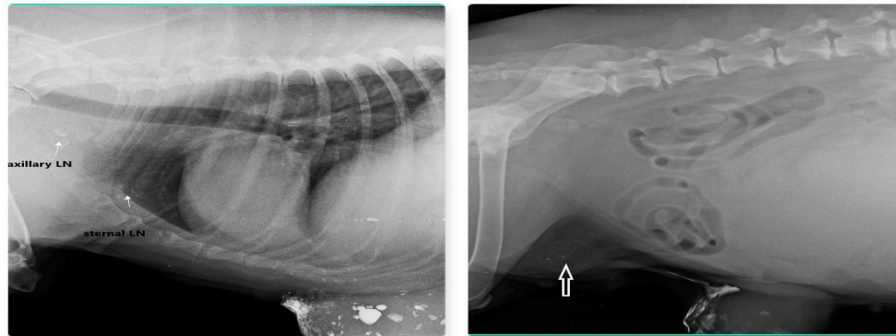
Figure 12. Sternal LN as SLN for carcinoma of 2nd and 3rd MG (left) and inguinal LN (arrow) as SLN for carcinoma of 4th and 5th MG (right) detected through indirect radiographic lymphography with Lipiodol.

Perioperative IL with MB dye was conducted under sedation within the operating room at the start of the surgery (radical mastectomy or lumpectomy), and blue stained inguinal lymph node (SLN for mammary carcinoma of 5th MG) was visible within 10-15 min as shown in Fig. 13.

Figure 13. IL with MB dye detect inguinal lymph node as SLN (stained blue) in mammary carcinoma of 5th mammary gland.

MB was employed in 12 procedures with the identification of 12 SLN (9 inguinal LN and three axillary LN). The lymph from the 2nd and 3rd mammary glands drains to the axillary and sternal LN, whereas the lymph from the 3rd, 4th, and 5th mammary glands flows to the inguinal lymph node and hind limb lymphoid plexus. Iohexol in indirect radiographic lymphography also detect SLN (inguinal LN) in 2 cases. Based on the cytology or histology of the excised LN, six nodes are found to be positive for metastases, while the remaining 17 echelon nodes are non-metastatic or non-malignant.

3.1. Automated Classification of Results and Analysis

Proposed automatic classification system is implemented on MATLAB® 2020a with 3.2GHz processor with 8GB RAM. The sample images of cropped regions are shown in Fig.14. Total six first-order statistical and fifteen GLCM features are extracted from all cropped regions and created feature set. Whole feature set is divided into 70% training and 30% testing set. SVM classifier with four kernel function namely, linear, polynomial, RBF, and MLP (Sigmoid) are used for classification. The various initial parameter values of SVM kernel functions taken for experiment are shown in Table 1.
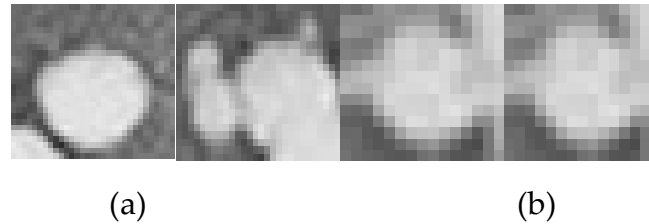
(a)   (b)

Figure 14. Cropped regions from X-ray images (a) Cancerous (b) Non-Cancerous.

Table 1. Parameter values of SVM kernel function.

Kernel function	Parameters values of Kernel Function
RBF	Sigma(σ)=1.2, Box Constrains (C) = 0.8
Polynomial	Poly-order = 4
MLP	Default-Scale with range of −1 to +1

The performance of SVM classifier is evaluated by computing accuracy, sensitivity, and specificity which are mathematically defined as:

Sensitivity, also called True Positive Rate (TPR), is defined as the ratio of the actual positive which are correctly classified as cancerous. It is also known as the true positive fraction (TPF).

$$Sensitivity = \frac{TP}{TP + FN} \tag{34}$$

Specificity, also called False Positive Rate (FPR), is defined as the ratio of the actual negative which are correctly classified as non- cancerous. It is also known as the false positive fraction (FPF).

$$Specificity = \frac{TN}{TN + FP} \tag{35}$$

Accuracy is defined as the ratio of the correct classification to the total number of test cases.

$$Accuracy = \frac{TP + TN}{TP + TN + FP + FN} \tag{36}$$

4. Discussion

Four types of IL approaches used in the current research methodology successfully detected 74 SLN in 82 diversified canine malignancies of epithelial origin (carcinomas) i.e. accounting for 90% of the cases, and simultaneously localize 7 SLN out of 14 tumors of mesenchymal origin (sarcomas) (7/14) i.e. 50%. Since the potential use of these dyes and contrast agents in soft tissue sarcoma cases is limited, the viability of the IL method in these cases is examined using MB dye, iohexol, and lipiodol. B-mode grayscale ultrasonography, and strain elastography are powerful tools in the detection of nodes (metastatic/non-metastatic) in these malignancies, which are confirmed by cytology, FNAC, or biopsy of the targeted nodes. Machine learning approach is also used to detect the carcinoma and spread of these cancerous tissue in multilevel extraction method.

IL approaches (Indirect CT lymphography with iohexol and IL with Lipiodol) can detect SLN for the first time in histiocytic sarcoma and buttock sarcoma, despite the fact that the majority of STS spread hematogenously and locally. This is consistent with earlier reports of Blazer *et al*. (2003), that regional LN metastasis is valuable only in 3-4 percent of STS as in rhabdomyosarcoma, epithelioid sarcoma, clear cell sarcoma, synovial sarcoma, and vascular sarcomas. The prognosis of buttock

sarcoma cases is poor due to detection of malignant nodes (SLN) whereas ultrasound guided biopsy of the anatomical lymph node in other STS reveals non-metastatic LN with favorable outcome.

Ipsilateral and Contralateral lymph node metastases are a common finding in the current investigation of canine oral and maxillofacial cancer (Grimes *et al*., 2017; Skinner *et al*., 2018; Randal *et al*., 2020). Patients with oral SCC showed identification of two lymphatic pathways from primary tumor masses at rostral mandible draining into two-echelon mandibular nodes (SLN), and cytology also revealed positive for metastasis. We have not observed that lymphadenectomy of the nodes positive for metastasis improve the OST in patient with oral SCC although it has modified clinical treatment and therapeutic intervention, comparable to findings by Skinner *et al*. 2017. Of the four IL techniques employed for SLN detection in our study, the Lipiodol-based IL methods has given better results than iohexol and MB as per the earlier report of Patsikas *et al*.2006, Mayer *et al*. 2013, and Brissot and Edery,2016. IL with MB is performed in two cases of ocular SCC where parotid lymphocentrum is identified as SLN in one case, which is confirmed to be metastatic, and have also tumor recurrence.

Lipiodol has a 100% detection rate when employed in 11 of 11 different neoplasms in the skin and subcutis. Cervical and popliteal LN is the first-tier node (SLN) for the forelimb and hind limb detected with both the IL techniques (Lipiodol and MB dye) respectively. The progress of Lipiodol through lymphatic and subsequent opacification of nodes take 24hours, compared to 2 minutes with iohexol, and 10-15 minute with MB dye.

Lipiodol has primarily used in our study for SLN mapping of ASAGAC and the medial iliac lymph node has recognized as SLN within 24h of injection and substantial contrast opacification is evident after 24h. The detection time and contrast enhancement are in line with other studies by earlier workers Majeski *et al*.2017, Liptak *and* Boston, 2019. Lymphadenomegaly was observed as mild in 4 cases, moderate in 1 case, and enlarged in 1 case. The size of the primary tumor mass (ASAGAC) is very large, measuring more than 2.5cm-10cm in length and 3-4cm diameter, and many of them showed lymphadenomegaly of at least one iliosacral LN (Sahoo *et al*., 2021b).

Lymphomas involving multiple nodes are involved in four cases, while popliteal LN and mediastinal mass are enlarged in one case each. All lymphomas shared the characteristic ultrasonography finding of rounded hypoechoic nodes with a S/L axis ratio 1. Cytology of the nodes is an essential criterion for the diagnostic of malignant lymphoma. Iohexol, both in radiography and CT, shows a 100 % detection rate (6 SLN in 5 cases), and lymphatic along with nodal opacification occurred within 2 minutes of injection. As most cases are multicentric involving several nodes and organs, the onset of the lesion may be traced to one site (for example- last molars in oral cavity and hyperemia of the eye in one case) based on clinical presentation and patient history. Sacral and iliac lymph nodes were identified as SLN in multicentric lymphoma with ocular involvement. The prognosis and OST in multicentric lymphoma are very poor, with less than three months of OST as observed by Falk, 2018. Canine lymphoma is similar in its clinical representation to human Non-Hodkinson's lymphoma. Further studies with a greater population of dogs will add to the therapeutic regimen in the human patient. IL with iohexol and MB was used for detection of SLN in TVT and mixed germ cell-stromal tumor. MB effectively localizes the lymphatic route draining from primary tumor mass to the superficial and deep inguinal LN (SLN), which was found positive for metastases. In TVT, inguinal LN is the SLN which is non-malignant on cytology.

The lymph drainage pattern and SLN found in the mammary carcinoma detected through Lipiodol ultra-fluid and MB are congruent with earlier reports (Chiorean*et al*., 2016; Lee *et al*., 2018; Manfredi *et al*., 2021). Timing of radiograph are zero (0),2, 5,30,60 min and 2, 24 and, 72 hours interval same as in Patsikas *et al*.2006 but further drainage to second-tier nodes as in Collivignarelli *et al*.2021 is because captured images at 24h interval with the subcutaneous route. Lymphatic drainage of Lipiodol through the intradermal route is found faster than the subcutaneous route, indicating lymph flow faster through the intradermal route than the subcutaneous route. Thoracic metastasis was observed in mammary carcinoma of 4th MG, where inguinal LN is detected as the SLN with Lipiodol. Therefore, the reason for pulmonary metastasis in this patient might be lymphatic flow from inguinal LN to iliosacral lymphocenter and from there to cisterna chyli, next to thoracic lymphatic ducts and

finally drains to the thorax producing metastasis. The detection rate of SLN with Lipiodol and MB was 100% (21/21), confirming the sensitivity and specificity of these two dyes in clinical cases of breast cancer both in companion animals and human beings. The reason for the 100 % detection rate of Lipiodol in these cases and also other IL techniques employed in our study is that this lymphotropic agent stayed in the lymph node for a longer period, and because of its oil base, it did not disperse into the interstitial space quickly or flow into the excretory system. Contrary to iohexol, which is excreted through the kidney, Lipiodol is mainly metabolized in the liver and stays in the liver for many days. In the present study, the proportion of metastatic to non-metastatic nodes was found to be 36/38 (94%) in a population of 96 patients indicates importance of the IL procedure in identification of exact nodes that may harbor the malignant cells. The chances of survival are higher in patients in which non-metastatic LN are biopsied or removed than the canine patients in which metastatic LN are detected and removed. This indicates metastatic SLN is a poorer prognostic indicator in any neoplasm in agreement with Liptak and Boston, 2019.

4.1. Performance assessment of machine learning classifier model

The outcome obtained with SVM classifier with four different kernel function namely, linear, MLP, Polynomial, and RBF are shown in Table 2

Table 2. Classification performance of the proposed system with different kernel functions.

Kernel function	Sensitivity (%)	Specificity (%)	Accuracy (%)
Linear	91.73	91. 29	91.86
MLP	79.23	89.13	82.31
Polynomial	90.95	91.91	91.63
RBF	**95.53**	**94.64**	**93.05**

The highest 95.53% sensitivity, 94.64% specificity, 93.05% accuracy are observed with RBF kernel function. Performance of the SVM classifier with RBF kernel function is better as compared to linear, polynomial, and MLP functions. Highest obtained testing accuracy is 93.05% shows that performance of SVM classifier is reliable. It is concluded from the result that trained machine learning model is robust for automatic detection of cancerous and non-cancerous regions of animal's images.

5. Conclusions

The patient's survival time is less in groups where metastatic SLN has removed; it might be due to lymphatic spread of the tumor or metastasis had already occurred before the procedure is employed. The authors recommend the inclusion of a SLN detection procedure in all types of malignancies for better prognosis and survival outcomes of the disease. Machine learning technique is also applied for automatic classification of cancerous tissues. Automatic detection system will helpful for the doctors to take second thoughts. In future, more robust and QoS based machine learning model will be developed with extended number of images.

Conflict of Interest: There is no conflict of interest.

Ethical Statement: The retrospective cases were approved in Institutional Animal Ethical Committee (IAEC), College of Veterinary Science and AH, OUAT. All the procedure was performed through written consent from patient owner and postoperative of the animals were taken care of at owner's residence. The excised samples collected and lymphography technique followed were as per the established protocol from cited literature.

References

1. Beer, P., Pozzi, A., Rohrer, B.C., Bacon, N., Pfammatter, N.S., Venzin, C.2018. The role of sentinel lymph node mapping in small animal veterinary medicine: A comparison with current approaches in human medicine. *Veterinary Comparative Oncology* **16**(2),178-187.

2. Beer, P., Rohrer-Bley, C. and Nolff, M.C.2022. Near-infrared fluorescent image-guided lymph node dissection compared with locoregional lymphadenectomies in dogs with mast cell tumors. *Journal of Small Animal Practice* 63,670-678. https://doi.org/10.1111/jsap.13529

3. Blazer, D.G., Sabel, M.S., Sondak, V.K.2003. Is there a role for sentinel lymph node biopsy in the management of sarcoma? *Surgical Oncology***12**(3), 201-206.

4. Brissot, H.N. and Edery, E.G.2016. Use of indirect lymphography to identify sentinel lymph node in dogs: a pilot study in 30 tumors. *Veterinary Comparative Oncology***15,**740–753.

5. Chiorean, L., Cui, X.W., Klein, S.A., Budjan, J., Sparchez, Z., Radzina, M., Jenssen, C., Dong, Y., Dietrich, C.F.2016. Clinical value of imaging for lymph nodes evaluation with particular emphasis on ultrasonography. *Z Gastroenterology* **54**(8),774-90. doi: 10.1055/s-0042-108656.

6. Collivignarelli, F., Tamburro, R., Aste ,G., Falerno, I., Del Signore, F., Simeoni, F., Patsikas, M., Gianfelici, J., Terragni, R., Attorri, V., Carluccio, A., Vignoli. M.2021. Lymphatic Drainage Mapping with Indirect Lymphography for Canine Mammary Tumors, *Animals***11,**1115.

7. Cortes C., Vapnik V., Support-vector networks, Machine learning 20(3) (1995) 273-297.

8. Elliker, K. R., Sommerville, B. A., Broom, D. M., Neal, D. E., Armstrong, S., & Williams, H. C. (2014). Key considerations for the experimental training and evaluation of cancer odour detection dogs: lessons learnt from a double-blind, controlled trial of prostate cancer detection. BMC urology, 14(1), 1-9.

9. Falk Elin. 2018. Prognosis of malignant lymphoma in dogs and correlation to thymidine kinase (TK1) : a retrospective study. Second cycle, A2E. Uppsala: *SLU, Dept. of Clinical Sciences*,1-39.

10. Fournier, Q., Cazzini, P., Bavcar, S.2018. Investigation of the utility of lymph node fine-needle aspiration cytology for the staging of malignant solid tumors in dogs. *Veterinary Clinical pathology***47,**489–500.

11. Fournier, Q., Thierry, F., Longo, M. *et al*.2020. Contrast-enhanced ultrasound for sentinel lymph node mapping in the routine staging of canine mast cell tumors: A feasibility study. *Veterinary Comparative Oncology,*1–12. https://doi.org/ 10.1111/vco.12647

12. Garcia-Uribe, A., Erpelding, T.N., Krumholz, A., *et al*.2015. Dual-Modality Photoacoustic and Ultrasound Imaging System for Noninvasive Sentinel Lymph Node Detection in Patients with Breast Cancer. *Science Reporter***5,**15748.

13. Gelb, H.R., Freeman, L.J., Rohleder, J.J., Snyder, P.W.2010. Feasibility of contrast enhanced ultrasound-guided biopsy of sentinel lymph nodes in dogs. *Veterinary Radiology & Ultrasound***51,** 628–633.

14. Grimes, J.A., Secrest, S.A., Northrup, N.C., Saba, C.F., Schmiedt, C.W.2017. Indirect computed tomography lymphangiography with aqueous contrast for evaluation of sentinel lymph nodes in dogs with tumors of the head. *Veterinary Radiology and Ultrasound* **58** (5), 559-564.

15. Hlusko, K.C., Cole, R., Tillson, D.M., *et al*.2020. Sentinel lymph node detection differs when comparing lymphoscintigraphy to lymphography using water soluble iodinated contrast medium and digital radiography in dogs. *Veterinary Radiology and Ultrasound***61,** 659– 666,. https://doi.org/10.1111/vru.12908

16. Haralick, R.M., Shanmugam, K., Dinstein, I.H. Textural features for image classification, IEEE Transaction on Systems, Man and Cybernetics 3(6), (1973) 610-621.

17. Iida, G., Asano, K., Seki, M., Ishigaki, K., Teshima, K., Yoshida, O., Edamura, K. and Kagawa, Y. 2013. Intraoperative identification of canine hepatocellular carcinoma with indocyanine green fluorescent imaging. *Journal of Small Animal Practice***54,** 594-600. https://doi.org/ 10.1111/ jsap. 12148

18. Jain, R., Dandekar, P., Patravale, V.2009. Diagnostic nanocarriers for sentinel lymph node Imaging. *Journal of Controlled Release***38**(2),90- 102.

19. Karakitsou, V., Christopher, M.M., Meletis, E., Kostoulas, P., Pardali, D., Koutinas, C.K., Mylonakis, M.2022. A comparison of cytologic quality in fine-needle specimens obtained with and without aspiration from superficial lymph nodes in the dog. *Journal of Small Animal Practice* 63: 16-21. https://doi.org/10.1111/jsap.13429

20. Kumar, A., Singh, S. K., Saxena, S., Lakshmanan, K., Sangaiah, A. K., Chauhan, H., &Singh, R. K. (2020). Deep feature learning for histopathological image classification of canine mammary tumors and human breast cancer. Information Sciences, 508, 405-421.

21. Lapsley, J., Hayes, G.M., Janvier, V., *et al*.2020. Influence of locoregional lymph node aspiration cytology vs sentinel lymph node mapping and biopsy on disease stage assignment in dogs with integumentary mast cell tumors. *Veterinary Surgery,*1–9. https://doi.org/10. 1111/vsu.13537

22. LeBlanc, A.K., Peremans, K.2014. PET and SPECT imaging in veterinary medicine. *Seminars in Nuclear Medicine* **44**(1),47-56. doi: 10.1053/j.semnuclmed.2013.08.004. PMID: 24314045.

23. Lee, C.E., Matz, B.M., Cole, R.C., Boothe, H.W., Tillson, D.M.2018. Radiographic evaluation of subcutaneously injected, water-soluble, iodinated contrast for lymphography in dogs.1-19. Doi.10.1101/325183.

24. Liptak, J.M., Boston, S.E.2019. Nonselective Lymph Node Dissection and Sentinel Lymph Node Mapping and Biopsy. *Veterinary Clinics of North America: Small Animal Practice***49,**793-807.

25. Majeski, S.A., Steffey, M.A., Fuller, M., Hunt, G.B., Mayhew, P.D., Pollard, R.E.2017. Indirect computed tomographic lymphography for iliosacral lymphatic mapping in a cohort of dogs with anal sac gland adenocarcinoma: technique description. *Veterinary Radiology Ultrasound***58** (3), 295-303.

26. Manfredi, M., De Zani, D., Chiti, L.E., *et al*.2021. Preoperative planar lymphoscintigraphy allows for sentinel lymph node detection in 51 dogs improving staging accuracy: feasibility and pitfalls. *Veterinary Radiology Ultrasound***62,** 602–609. https://doi.org/10.1111/vru.12995

27. Materka, A, Strzelecki, M. Texture analysis methods–a review, Technical University of Lodz, Institute Of Electronics, COST B11 report, Brussels, 1998, pp. 9-11.

28. Morton, D.L., Wen, D., Wong, J.H.1992. Technical details of intraoperative lymphatic mapping for early stage melanoma. *Archaeology of Surgery***127,**392–399.

29. Nyberg, R.H., Korkola, P., Maenpaa, J.2011. Ovarian sentinel node: is it feasible? *International journal of Gynaecology and Cancer***21**(3),568–72.

30. Patnaik, A., Ehler, W., MacEwen, E.1984. Canine cutaneous mast cell tumor: morphologic grading and survival time in 83 dogs. *Veterinary Pathology***21,** 469-474.

31. Patsikas, M.N., Karayannopoulou, M., Kaldrymidoy, E., *et al*.2006. The Lymph Drainage of the Neoplastic Mammary Glands in the Bitch: A Lymphographic Study. *Anatomia, histologia, embryologia***35,** 228-34.

32. Randall, E.K., Jones, M.D., Kraft, S.L., Worley, D.R.2020. The development of an indirect computed tomography lymphography protocol for sentinel lymph node detection in head and neck cancer and comparison to other sentinel lymph node mapping techniques. *Veterinary Comparative Oncology***18**(4),634-644.

33. Rossi, F., Korner, M., Suarez, J.2018. Computed tomographic lymphography as a complementary technique for lymph node staging in dogs with malignant tumors of various sites. *Veterinary Radiology Ultrasound* **59,**155–162.

34. Sahoo AK, Nath I, Senapati SB, Panda SK, Das MR. and Patra BK. 2021a. Comparative Evaluation of Nutraceuticals (*Curcuma longa* L., *Syzygium aromaticum* L. and *Olea europaea*) with Single-agent Carboplatin in the Management of Canine Appendicular Osteosarcoma. Indian Journal of Animal Research. DOI: 10.18805/IJAR.B-4485

35. Sahoo, A.K., Nath, I., Senapati, S.B., Panda, S.K., Das, M.R., Patra, B.K.2021b. Apocrine Gland Anal Sac Adenocarcinoma in Dogs: 22 Cases (2015-2020). *Indian Journal of Animal Research,*1-6. DOI: 10.18805/IJAR.B-4371

36. Sarowitz, B.N., Davis, G.J. and Kim, S.2017. Outcome and prognostic factors following curative-intent surgery for oral tumors in dogs: 234 cases (2004 to 2014). *Journal of Small Animal Practice* 58, 146-153. https://doi.org/10.1111/jsap.12624

37. Shaker, R., Wilke, C., Ober, C., & Lawrence, J. (2021). Machine learning model development for quantitative analysis of CT heterogeneity in canine hepatic masses may predict histologic malignancy. Veterinary Radiology & Ultrasound, 62(6), 711-719.

38. Skinner,O.T., Boston, S.E., Souza, C.H.M.2017. Patterns of lymph node metastasis identified following bilateral mandibular and medial retropharyngeal lymphadenectomy in 31 dogs with malignancies of the head, *Veterinary Comparative Oncology***15**(3), 881-889.

39. Skinner, O.T., Boston, S.E., Giglio, R.F.2018. Diagnostic accuracy of contrast enhanced computed tomography for assessment of mandibular and medial retropharyngeal lymph node metastasis in dogs with oral and nasal cancer. *Veterinary Comparative Oncology***16,** 562–570.

40. Sledge, D. G., Webster, J., &Kiupel, M. 2016. Canine cutaneous mast cell tumors: A combined clinical and pathologic approach to diagnosis, prognosis, and treatment selection. *The Veterinary journal 215*, 43–54. https://doi.org/10.1016/j.tvjl.2016.06.003

41. Turkbey, B., Hoyt, R.F., Jr Agarwal, H.K., *et al*.2015. Magnetic resonance sentinel lymph node imaging of the prostate with gadofosveset trisodium-albumin: preliminary results in a canine model. *Academic radiology***22**(5), 646–652.

42. Wan, J., Oblak, M.L., Ram, A., Singh, A., Nykamp, S.2021. Determining agreement between preoperative computed tomography lymphography and indocyanine green near infrared fluorescence intraoperative imaging for sentinel lymph node mapping in dogs with oral tumors. *Veterinary Comparative Oncology*19, 295– 303. https://doi.org/10.1111/vco.12675

disclaim responsibility for any injury to people or property resulting from any ideas, methods, instructions or products referred to in the content.